
Since January 2020 Elsevier has created a COVID-19 resource centre with free information in English and Mandarin on the novel coronavirus COVID-19. The COVID-19 resource centre is hosted on Elsevier Connect, the company's public news and information website.

Science of the Total Environment 795 (2021) 148877

Contents lists available at ScienceDirect

Science of the Total Environment

journal homepage: www.elsevier.com/locate/scitotenv

# Unveiling the changes in urban atmospheric $CO_2$ in the time of COVID-19 pandemic: A case study of Florence (Italy)

Stefania Venturi [a,b,*], Antonio Randazzo [a], Franco Tassi [a,b], Beniamino Gioli [c], Antonella Buccianti [a], Giovanni Gualtieri [c], Francesco Capecchiacci [a,b], Jacopo Cabassi [b], Lorenzo Brilli [c], Federico Carotenuto [c], Riccardo Santi [a], Carolina Vagnoli [c], Alessandro Zaldei [c], Orlando Vaselli [a,b]

[a] Department of Earth Sciences, University of Florence, Via G. La Pira 4, 50121 Firenze, Italy
[b] Institute of Geosciences and Earth Resources (IGG), National Research Council of Italy (CNR), Via G. La Pira 4, 50121 Firenze, Italy
[c] Institute for BioEconomy (IBE), National Research Council of Italy (CNR), Via G. Caproni 8, 50145 Firenze, Italy

## HIGHLIGHTS

- The outbreak of COVID-19 pandemic abruptly reduced $CO_2$ emissions at urban scale.
- A rapid response of $CO_2$ flux measurements in Florence was observed.
- $\delta^{13}C$-$CO_2$ values recorded the change in the prevailing urban $CO_2$ emitting sources.
- The daily $CO_2$ enhancement reflected changes in the strength of emitting sources.
- COVID-19 pandemic resulted in appreciable reductions of $CO_2$ levels in urban air.

## GRAPHICAL ABSTRACT

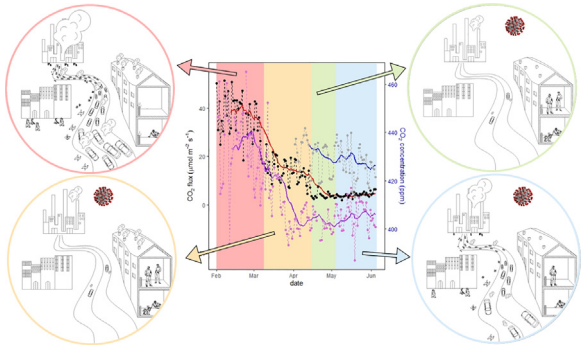

## ARTICLE INFO

*Article history:*
Received 17 April 2021
Received in revised form 10 June 2021
Accepted 2 July 2021
Available online 3 July 2021

Editor: Pavlos Kassomenos

*Keywords:*
COVID-19 pandemic
Greenhouse gas
$CO_2$
Urban air
Carbon footprint

## ABSTRACT

The outbreak of COVID-19 pandemic was accompanied by global mobility restrictions and slowdown in manufacturing activities. Accordingly, cities experienced a significant decrease of $CO_2$ emissions. In this study, continuous measurements of $CO_2$ fluxes, atmospheric $CO_2$ concentrations and $\delta^{13}C$-$CO_2$ values were performed in the historical center of Florence (Italy) before, during and after the almost two-month long national lockdown. The temporal trends of the analyzed parameters, combined with the variations in emitting source categories (from inventory data), evidenced a fast response of flux measurements to variations in the strength of the emitting sources. Similarly, the $\delta^{13}C$-$CO_2$ values recorded the change in the prevailing sources contributing to urban atmospheric $CO_2$, confirming the effectiveness of carbon isotopic data as geochemical tracers for identifying and quantifying the relative contributions of emitting sources. Although the direct impact of restriction measurements on $CO_2$ concentrations was less clear due to seasonal trends and background fluctuations, an in-depth analysis of the daily local $CO_2$ enhancement with respect to the background values revealed a progressive decrease throughout the lockdown phase at the end of the heating season (>10 ppm), followed by a net increase (ca. 5 ppm) with the resumption of traffic. Finally, the investigation of the shape of the frequency distribution of the analyzed variables revealed interesting aspects concerning the dynamics of the systems.



* Corresponding author at: Department of Earth Sciences, University of Florence, Via G. La Pira 4, 50121 Firenze, Italy.
*E-mail address:* stefania.venturi@unifi.it (S. Venturi).

https://doi.org/10.1016/j.scitotenv.2021.148877
0048-9697/

## 1. Introduction

The alarming spread and gravity of the Severe Acute Respiratory Syndrome Coronavirus-2 (SARS-CoV-2) infection led, on March 11, 2020, the World Health Organization (WHO) to declare the coronavirus (COVID-19) outbreak a global pandemic. Consequently, worldwide governments adopted strategic restrictive measures suppressing industrial and commercial activities, limiting human movements (including social distancing), in order to contain the diffusion of confirmed positive cases and number of deaths (Brauner et al., 2020; Haug et al., 2020). As a collateral effect, these restrictions produced a suite of indirect positive impacts on the environment, largely improving both water and air quality, as documented by recent literature (e.g. Abdullah et al., 2020; Adams, 2020; Baldasano, 2020; Berman and Ebisu, 2020; Dantas et al., 2020; Gualtieri et al., 2020; Khan et al., 2020; Kerimray et al., 2020; Li et al., 2020; Liu et al., 2020; Mahato et al., 2020; Otmani et al., 2020; Paital, 2020; Sharma et al., 2020; Tobías et al., 2020; Wang et al., 2020; Elsaid et al., 2021; Han et al., 2021). Similarly, a clear reduction in greenhouse gas (GHG) emissions due to COVID-related restrictions was observed, with a decrease in daily global $CO_2$ emissions at national scale ranging from 11 to 25% by April 2020 compared to 2019 levels (Le Quéré et al., 2020) and an overall drop in global $CO_2$ emissions of 6.4% (corresponding to 2.3 billion tons) in 2020 (Tollefson, 2021). On the other hand, the COVID-19-related $CO_2$ emission drop in May 2020 was estimated to account only for 0.4 ppm on the expected concentration of $CO_2$ in the atmosphere at a global scale (Betts et al., 2020), equivalent to a reduction of about 0.1%. Accordingly, the atmospheric $CO_2$ concentrations measured at the Mauna Loa Observatory (Hawaii, USA) increased by 0.7% (up to 416.21 ppm) in April 2020 compared with April 2019 (Tans and Keeling, 2020).

While at the global scale the COVID-related emission reductions were relatively small and the impact on GHG concentrations was hardly detectable, the pandemic-related restrictions had a disproportionate effect on atmospheric $CO_2$ at urban scale, where emission reductions were expected to be large and the impact on $CO_2$ concentrations detectable. It is well established that cities are responsible for ~70% of energy-related GHG emissions (Hoornweg et al., 2011), mostly related to housing and traffic sectors (Pichler et al., 2017), and their relevance in terms of $CO_2$ emissions driving global climate change is widely recognized (Duren and Miller, 2012; Baur et al., 2014). An ICOS report (Papale et al., 2020), where monitoring net emissions of $CO_2$ at neighborhood scale over several cities throughout Europe were described, showed that the reduction in urban $CO_2$ release to the atmosphere during lockdown ranged from 8 to 75%, as a function of the underlying urban activities and extension of urban green spaces. Turner et al. (2020) estimated a 30% drop in urban $CO_2$ emissions from the San Francisco Bay Area (California, USA), mostly related to changes in traffic. Similarly, Liu et al. (2021) evidenced a clear decrease and change in temporal patterns of on-road $CO_2$ concentrations in Beijing (China) due to the pandemic-related restrictions to urban mobility. Wu et al. (2021) estimated a decrease of 7.5% of atmospheric $CO_2$ concentrations in the urban area of Xi'an (China) during the lockdown period, although the relaxation of confinement measures rapidly re-established $CO_2$ levels similar to those observed in 2019. Accordingly, the COVID-19 outbreak and the related population confinement strategies have provided a unique, though unexpected, opportunity to empirically assess the effect of emissions cutting on urban $CO_2$ plume and the impact of the progressive resumption of urban normal functions at the end of the lockdown periods. Such information is crucial for assessing the actual impact of local policymakers' efforts to mitigate climate change (IPCC, 2018; Mitchell et al., 2018) and to test the effectiveness of the implementation of green technologies (e.g. Turner et al., 2020; Wu et al., 2021). Moreover, this critical juncture in the world history allowed to effectively assess emission changes (measured by eddy covariance) and source categories (inventory data) by looking at GHG isotopic and concentration values and local $CO_2$ enhancement with respect to background values. Nevertheless, to the best of our knowledge, no study has been published involving a comprehensive monitoring of urban $CO_2$ during the COVID-related lockdown, i.e. including flux, concentration and carbon isotope measurements.

In this study, we explored the real-time variation in atmospheric $CO_2$ and the isotopic carbon composition in the historical center of Florence (Italy), coupled with $CO_2$ flux measurements performed over the urban canopy, during and immediately after the heavy COVID-19 restrictions. Florence city center was selected based on two main reasons: (i) availability of a full dataset covering the whole study period, including observations of $CO_2$ concentrations, $CO_2$ fluxes, meteorological parameters, and carbon isotopic composition; (ii) the evidence, after Vaccari et al. (2013), that the contribution of urban vegetation to $CO_2$ fluxes over Florence city center is negligible, so that the origin of $CO_2$ emissions in the study area is fully anthropogenic. A comparison with the temporal variation in atmospheric $CH_4$ concentrations and carbon isotopic composition was also performed. The aims of this study were to: (i) assess the impact of national confinement on the urban $CO_2$ plume in terms of both fluxes and atmospheric concentrations; (ii) investigate the associated variations in the carbon isotopic signature of atmospheric $CO_2$; and (iii) analyze the response of urban $CO_2$ fluxes and concentrations to variations of anthropogenic emissions. The produced dataset offered insights on drivers and dynamics regulating the urban carbon cycle, contributing to fill knowledge gaps in the current understanding of anthropogenic and natural processes controlling the urban carbon footprint (e.g. Hutyra et al., 2014; Marcotullio et al., 2014; Mitchell et al., 2018) and providing indications to policymakers on where to direct efforts to achieve carbon neutrality.

## 2. Material and methods

### 2.1. Characteristics of the study area and timing of COVID-related measures

The study area was located in the city of Florence, in central Italy (Fig. 1). Italy was the first country in Europe adopting restrictions to counteract the COVID-19 infection outbreak. On March 9, 2020, the Italian Prime Minister issued the decree law informally named *#Iorestoacasa* (in Italian for "I stay at home") which established a national lockdown ("phase 1"), limiting movements for all the people with exception of documented work needs, emergencies or health reasons, promoting smart working and restricting recreational and commercial activities. After two months of national lockdown, the so-called "phase 2" started in Italy on May 4, 2020, progressively easing restrictions and allowing people to travel within their residence region. Accordingly, traffic progressively resumed, although the pre-lockdown levels did not completely restore due to the persistent closure of schools, universities, and most public offices and commercial activities, as well as the lack of tourism-related movements. Eventually, phase 3, in force since July 12, 2020, reduced limitations and restored the majority of industrial and commercial activities. The drastic travel restrictions imposed to some 60 million people and the stop to most of the economic activities during the national lockdown produced a considerable reduction of road traffic and, consequently, of short-term pollutants (e.g. $NO_2$, CO, $SO_2$, $C_6H_6$) levels in urban air (e.g. Collivignarelli et al., 2020; Tobías et al., 2020), as impressively depicted by satellite imagery (e.g. Bauwens et al., 2020; Zambrano-Monserrate et al., 2020) and registered by the air quality monitoring network managed by the Italian Environmental Agency (ARPA). Similarly, GHG emissions plummeted, with a reduction of the anthropogenic carbon footprint of 20% with respect to 2015–2018, corresponding to avoided GHG emissions in between ~5.6 and ~10.6 Mt $CO_2$ equivalents (Rugani and Caro, 2020). In Florence, the urban $CO_2$ emissions in March and April 2020 experienced a reduction of 45% compared to previous years (Papale et al., 2020).

The measurements were carried out in the highly urbanized city center of Florence (3683 inhabitants/$km^2$; Fig. 1), which is characterized by a network of streets and alleys and hosts residential, tertiary and

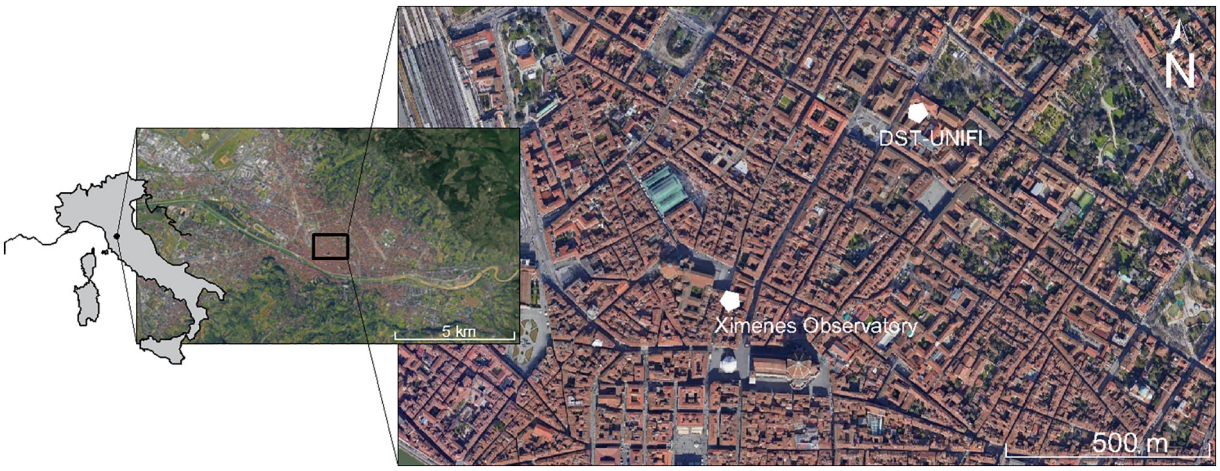


**Fig. 1.** Satellite images of (i) the metropolitan area and (ii) the historical center of Florence (Italy). The location of the monitoring sites (Ximenes Observatory and DST-Unifi) is shown (white pentagons).

commercial sectors. Differently, the industrial district is in the suburb of the city. Consequently, gas emissions in the city center are mainly deriving from vehicular traffic and domestic heating, accounting for about 35 and 65% of $CO_2$ emissions (Regione Toscana, 2010; Gioli et al., 2012, 2015; Venturi et al., 2020). According to the Italian regulations of condominium heating plants, the ignition of domestic heating is established on the basis of climatic zone (DPR no. 412 of 26/08/1993). In the city of Florence, a maximum of 12 h per day from Nov. 1st to Apr. 15th is allowed for residential heating usage.

Overall, the data presented in this study encompassed the period from before the forced confinement time to the easing of restrictions in spring 2020. In particular, the monitored period can conveniently be subdivided into 4 sub-intervals, i.e. (i) the pre-COVID phase (hereafter, "*PRE*"), including data acquired before the onset of the national lockdown (i.e. until March 8, 2020), (ii) the lockdown phase from March 9 to April 15 (hereafter, "*LH*"), when domestic heating was active and mobility restrictions were in force, (iii) the lockdown period from April 16 to May 3 (hereafter, "*LN*"), i.e. when domestic heating was switched off but mobility restrictions persisted, and (iv) the onset of phase 2 (hereafter, "*P2*"), started on May 4, when mobility restrictions were progressively lifted.

### 2.2. Measurements of $CO_2$ fluxes, concentrations and carbon isotopic composition

Turbulent fluxes of energy, momentum and $CO_2$ were measured with the eddy covariance (EC) technique at half-hourly resolution from the equipment positioned on the roof of the Ximenes Observatory (43° 47′ N, 11° 15′ E; Fig. 1), located in a pedestrianized area of the city center, ca. 33 m above the ground level and 18 m above the average building height. A three-dimensional sonic anemometer (Metek USA-1, Metek GmbH, Elmshorn Germany), and a $CO_2$ and $H_2O$ open-path infrared gas analyzer (Licor LI-7500A, Li-Cor Inc., Lincoln, Nebraska, USA) were logged at the frequency of 20 Hz and fluxes were computed by means of the EddyPro software package (Li-Cor Inc., https://www.licor.com/env/support/EddyPro/software.html). Within the software package, raw data were treated with appropriate corrections, such as despiking of gas analyzer data (Vickers and Mahrt, 1997), high-pass filtering with linear detrending and coordinate axis rotation (Aubinet et al., 2000) and corrections for air density fluctuations (Webb et al., 1980). Quality-control procedures were applied according to Foken and Wichura (1996) procedure. Single point storage correction was applied as described in Papale et al. (2006). More detail on the experimental setup at this site can be found in Gioli et al. (2015). Moreover, standard meteorological parameters were acquired with a weather station. Both EC and weather station were active since 2005. In the framework of this study, data from February 1 to June 4, 2020, were collected.

Concentrations and carbon isotopic compositions of $CO_2$ and $CH_4$ ($\delta^{13}C$-$CO_2$ and $\delta^{13}C$-$CH_4$, expressed in ‰ vs. V-PDB) in air were continuously measured at the Department of Earth Science at University of Florence (DST-Unifi, 43° 46′ N; 11° 15′ E; Fig. 1), ca. 550 m away from the Ximenes Observatory and along a generally lightly trafficked road, using a Picarro G2201-i cavity ring-down spectrometer (CRDS) instrument. Measurements were performed from April 2 to June 4, 2020, with a one-second frequency. The Picarro analyzer was housed inside the Laboratory of Fluid Geochemistry at the Department of Earth Sciences of Florence (DST-Unifi) and connected through a Teflon tube to the outdoor, i.e. the internal courtyard of DST-Unifi. The tube was fixed at a height of 2 m above the ground level. The precision was within 0.2 and 0.05 ppm for $CO_2$ and $CH_4$ concentrations, respectively, and 0.16 and 1.15‰ vs. V-PDB for $\delta^{13}C$-$CO_2$ and $\delta^{13}C$-$CH_4$, respectively.

### 2.3. Urban mobility and natural gas consumption by domestic heating amounts

Urban road mobility data were collected from the online platform developed by EnelX Italia LLC and Here Technologies (EnelX and Here, 2020), where traffic flows from February 17 to June 4, 2020, were expressed as daily normalized variations with respect to a standard reference period, i.e. to the weighted average of the flows recorded from January 13 to February 16, 2020, assumed as a baseline mobility condition prior to the onset of COVID-19-related restrictions.

Daily variations in natural gas consumption by domestic heating were provided by Estra Ltd. for the period from February 1 to June 4, 2020, and were expressed as daily normalized variations with respect to the monthly average gas consumption during January 2020.

### 2.4. Explorative and statistical methods

Data reduction (hourly and daily averages and rolling averages; see below) and analysis were carried out using R (R Core Team, 2017) implemented with the Openair package (Carslaw and Ropkins, 2012; Carslaw, 2014) and Matlab R2020b licensed to the University of Florence. The acquired data were referred to local time, i.e. CEST (Central European Summer Time). The daily cycles of the measured variables were obtained through the Openair package from the average values per each hour of the day; the 95% confidence interval was also

calculated to take into account the variability of the measured parameters (Carslaw, 2014).

In order to smooth out short-term erratic fluctuations of measured values related to transient effects, e.g. (i) sudden changes of meteorological conditions, (ii) weekly variations in emitting sources, or (iii) fortuitous external factors, 15 days rolling-averages were considered. The latter were calculated for each day as the average of the previous 15 days (e.g. the 15 days rolling average referred to April 17 represented the average of daily values from the interval April 3 to 17). The selected time interval approximately corresponded to the duration of *LH* and *LN* observation periods, allowing to investigate the impact of domestic heating season and COVID-19-related restrictions on the measured parameters.

The explorative analysis was followed by the investigation of the dynamics of the measured variables by using distributional analysis to probe the resilience to change, presence of alternative states, autocorrelation in time (Scheffer et al., 2012). The key idea is that the shape of the probability density function describing the behavior of the variables is able to give information about governing dynamics of the system (van Rooij et al., 2013). In this framework, the dynamics of the systems was categorized in component-dominant dynamics and interaction-dominant dynamics (Holden et al., 2009; Holden and Rajaraman, 2012). In the first case, the event-distributions reflect the activity of isolable components, their time-course and an unsystematic additive source of noise. By contrast, in the second case coordination and coupling among processes emerge, so that interactions play a fundamental role generative multiplicative and cascade effects. The distributional analysis was performed on half-hourly averaged $CO_2$ fluxes and on one-second data for $CO_2$ concentrations and $\delta^{13}C$-$CO_2$ values.

## 3. Results

The daily-averaged urban $CO_2$ fluxes showed a first sharp decrease from *PRE* (median value of 37.1 μmol $m^{-2}$ $s^{-1}$) to *LH* (median value of 13.3 μmol $m^{-2}$ $s^{-1}$) phase, and a second drop after the end of the heating season, i.e. during *LN* phase (median value of 3.51 μmol $m^{-2}$ $s^{-1}$). A small increase in EC flux measurements was observed during *P2* phase, when, however, $CO_2$ fluxes (median value of 4.05 μmol $m^{-2}$ $s^{-1}$) remained one order of magnitude lower than those measured during the *PRE* phase. A similar trend was observed in the daily-averaged $CO_2$ concentrations measured by the EC monitoring station, with the highest values being recorded during the *PRE* phase (with a median value of 434 ppm), followed by a sharp drop during the *LH* phase (with a median value of 407 ppm) and a minor decrease during the *LN* phase (with a median value of 402 ppm), whereas the onset of the *P2* phase was characterized by a slight increase in $CO_2$ concentrations (with a median value of 406 ppm).

The daily-averaged $CO_2$ concentrations measured by the Picarro analyzer at the street level showed a slight decrease (i.e. few ppm) throughout the whole observation period, with median values of 435.5, 431.8 and 427.9 ppm in the *LH*, *LN* and *P2* phases, with values ranging from 420.1 to 441.8 ppm, from 418.9 to 435.6 ppm and from 413.1 to 439.8 ppm, respectively. Conversely, the $\delta^{13}C$-$CO_2$ values showed an overall increase, ranging from −12.1 to −10.7‰ vs. V-PDB, from −11.7 to −10.6‰ vs. V-PDB and from −11.4 to −9.75‰ vs. V-PDB in the *LH*, *LN* and *P2* phases, with median values of −11.7, −11.3 and −10.6‰ vs. V-PDB, respectively.

The daily-averaged $CH_4$ concentrations displayed a small decrease (<0.1 ppm) throughout the whole monitoring period, with median values of 2.06, 2.05 and 2.04 ppm during the *LH*, *LN* and *P2* phases, with values oscillating, respectively, from 1.99 and 2.09 ppm, from 1.99 to 2.08 ppm, and 1.98 and 2.08 ppm. The $\delta^{13}C$-$CH_4$ values increased from a median value of −48.1‰ vs. V-PDB during the *LH* phase, to −47.5 and −47.1‰ vs. V-PDB in the *LN* and *P2* phases, respectively, with values from −48.5 and −47.6‰ vs. V-PDB, from −48.6 to −47.2‰ vs. V-PDB and from −47.4 to −46.5‰ vs. V-PDB, respectively.

## 4. Discussion

### 4.1. Temporal variations of urban road mobility and natural gas consumption

The adoption of confinement measures to control the COVID-19 pandemic produced an abrupt reduction in the urban road mobility in Florence, as shown in Fig. 2A. Even before the national lockdown imposed by the *#Iorestoacasa* decree law, the data registered a sensible decrease in the road traffic, likely due to reductions in tourism flows. However, after March, 9, when Italians were forced to stay at home, road traffic dropped sharply and rapidly, with a reduction of ca. 65% with respect to pre-COVID levels. On the other hand, despite the persistence of school closures and limits on interregional movements, urban traffic flows rapidly increased after the end of the confinement time, reaching values higher than 60% of pre-COVID traffic levels after May 18, with the sole exception of a temporary reduction of road mobility related to the Italian national holiday of June 2 (Republic Day). It has to be considered that the pandemic likely changed the citizens' travel habits, such as a significant reduction of the public transportation due to the risk of contagion and a relative increase of private means of transport, including environmental sustainable vehicles, e.g. bicycles and electric scooters favored by the pleasant spring weather, but also private cars (Lozzi et al., 2020).

As evidenced by data provided by Estra Ltd., the natural gas consumption appeared to be mainly driven by domestic heating controlled by climate conditions, as clearly results from the comparison of temporal trends in daily-averaged natural gas demand (Fig. 2B) and air temperatures (Fig. 2C) which displayed a strong negative correlation (non-parametric Spearman's correlation coefficient $r = -0.94$). A drastic cut in the natural gas demand was recorded during the first half of April 2020, i.e. at the end of the heating season and corresponding to a progressive increase in air temperatures, when gas consumption dropped from >60% with respect to the standard reference period to less than 30%. A stabilization at ca. 14% with respect to January levels was observed from the beginning of May to June 4, which was mostly attributable to gas consumption due to cooking and water heating. The diurnal pattern of natural gas consumption (Fig. 2D) experienced as expected a higher demand during daytime. Notably, three peaks occurred when the domestic heating systems were on, i.e. at ca. 06–08, 12 and 18–20. The morning and evening peaks were more pronounced during the *PRE* and *LH* phases, whereas the three peaks were comparable and hardly distinguishable from the diurnal baseline during the *LN* and *P2* phases, confirming the drop of natural gas consumption at the end of the heating season.

### 4.2. Temporal variations in the carbon isotopic fingerprint of atmospheric $CO_2$

The change in urban $CO_2$ emitting sources in response to both confinement provisions and seasonality was expected to produce a change in the carbon isotopic signature of $CO_2$ in urban air. In fact, $CO_2$ emissions from natural gas combustion and vehicular traffic are characterized by distinguishable carbon isotopic compositions, i.e. from −44 to −37‰ vs. V-PDB (e.g. Clark-Thorne and Yapp, 2003; Widory and Javoy, 2003; Chamberlain et al., 2016; Pang et al., 2016) and ca. −27‰ vs. V-PDB (e.g. Clark-Thorne and Yapp, 2003; Widory and Javoy, 2003; Zimnoch, 2009; Górka and Lewicka-Szczebak, 2013; Pang et al., 2016), respectively. Once released in the atmosphere, the emitted gas mixes with background $CO_2$, which is characterized by a markedly higher isotopic ratio (i.e. −8.6‰ vs. V-PDB, as annual average measured in 2019 at Mauna Loa Observatory; Keeling et al., 2005). Actually, the measured $\delta^{13}C$-$CO_2$ values (from −12.1 to −9.75‰ vs. V-PDB) were intermediate between those anthropogenic sources and background values. As shown in Fig. 3A, the daily averages of $\delta^{13}C$-$CO_2$ values showed an overall increasing trend during the observation period, with a flattening

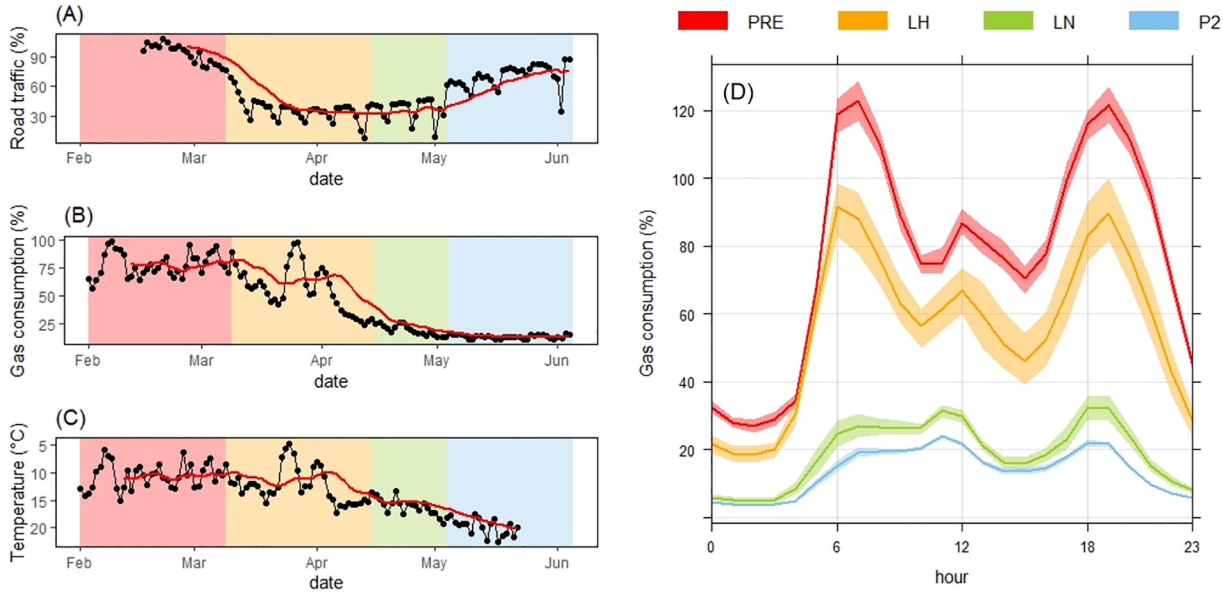


**Fig. 2.** (A) Road traffic (in %), (B) natural gas consumption (in %) and (C) temperature (in °C, in reverse scale) variations. Road mobility and natural gas consumption were normalized as described in the text. The colored areas refer to *PRE* (red), *LH* (orange), *LN* (yellow) and *P2* (cyan) phases. (D) Diurnal cycle of natural gas consumption (in %), normalized as described in the text, during *PRE* (red curve), *LH* (orange curve), *LN* (yellow curve) and *P2* (cyan curve) phases. The shaded areas represent 95% confidence intervals.

around −10.5‰ vs. V-PDB starting from the second half of May, which could be ascribed to a progressive decrease in the amount of non-background $CO_2$ in air as well as to a change in the isotopic composition of the emitted $CO_2$. To verify this hypothesis, a Keeling plot analysis (Keeling, 1958, 1961) was performed on the measured data in order to assess the temporal evolution of the carbon isotopic signature of

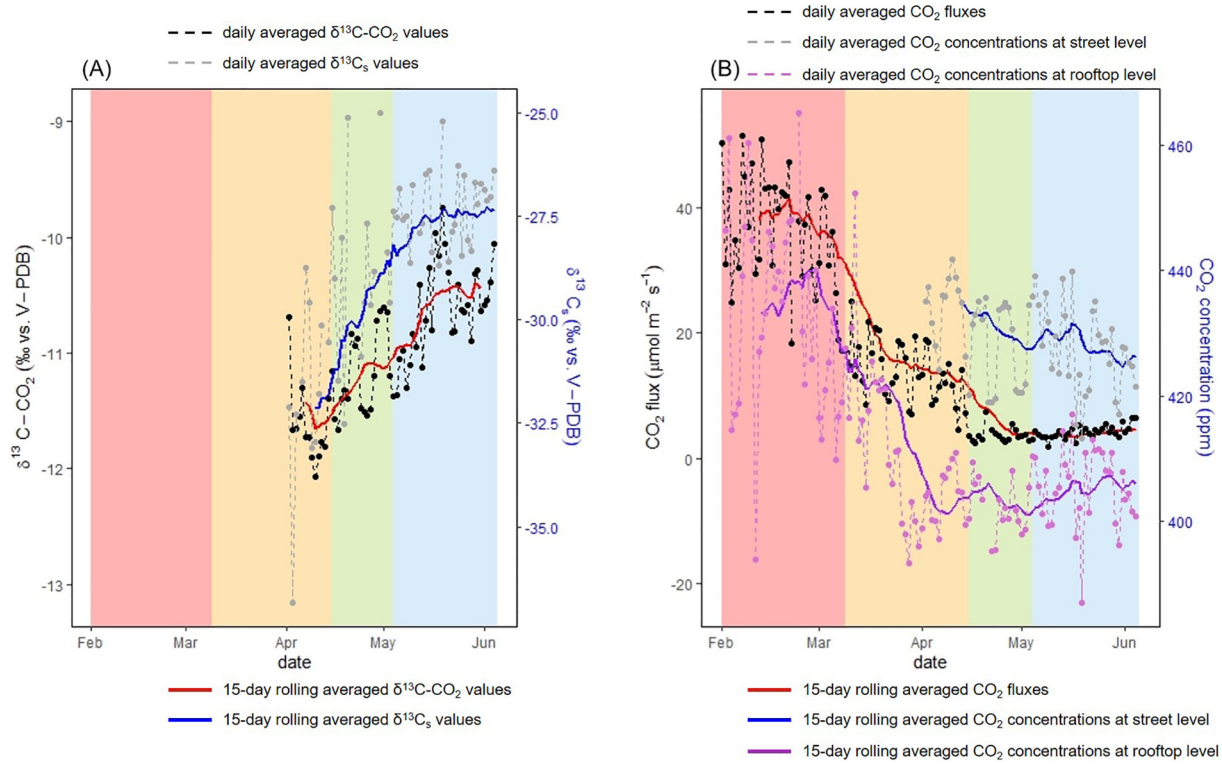


**Fig. 3.** (A) Temporal pattern of $\delta^{13}C$-$CO_2$ values, expressed as daily averages (black dashed curve) and 15-day rolling averages (red curve). The $\delta^{13}C_s$ values resulting from the Keeling plot analysis, expressed as daily averages (grey dashed curve) and 15-day rolling averages (blue curve), are also reported. (B) Temporal pattern of (i) $CO_2$ fluxes (in μmol $m^{-2}$ $s^{-1}$), expressed as daily averages (black dashed curve) and 15-day rolling averages (red curve), (ii) $CO_2$ concentrations (in ppm) measured at street level at DST-Unifi and expressed as daily averages (grey dashed curve) and 15-day rolling averages (blue curve), and (iii) $CO_2$ concentrations (in ppm) measured at roof level at Ximenes Observatory and expressed as daily averages (orchid dashed curve) and 15-day rolling averages (purple curve). The colored areas refer to *PRE* (red), *LH* (orange), *LN* (yellow) and *P2* (cyan) phases.

$CO_2$ emitted from the urban sources ($\delta^{13}C_s$, in ‰ vs. V-PDB). According to this method, the $\delta^{13}C_s$ values were calculated from the measured $CO_2$ concentrations and $\delta^{13}C$-$CO_2$ values as the intercept of the data regression line on a $\delta^{13}C$-$CO_2$ vs. $1/CO_2$ binary plot (not shown) by adopting a series of quality criteria, i.e. considering (i) 5 h intervals of monotonous increase of hourly-averaged $CO_2$ concentrations, (ii) a $r^2$ threshold of 0.75 and (iii) an intercept standard error limit of 2‰ (e.g. Pataki et al., 2003a, 2003b; Chamberlain et al., 2016; Vardag et al., 2016; Venturi et al., 2020). The resulting $\delta^{13}C_s$ values, representing the carbon isotopic signature of the non-background $CO_2$, expressed as both (i) daily averages (grey dashed curve) and (ii) 15-day rolling averages (blue curve), ranged from −36.8 to −25.0‰ vs. V-PDB, with a progressive increase from ca. −32.1‰ in *LH* to ca. −27.2‰ at the end of May and the beginning of June (Fig. 3A), confirming an evolution in the isotopic composition of the $CO_2$ emitted in the urban area. In particular, the obtained temporal trend highlighted the rapid response of carbon isotopic data to changes in emitting sources, i.e. from a relevant though progressively $CO_2$ decreasing input to the atmosphere from natural gas combustion during the *LH* phase to a largely prevailing traffic-derived $CO_2$ during the *P2* phase.

### 4.3. Temporal patterns of urban $CO_2$ fluxes

While isotopic data revealed a drastic change in the origin of urban atmospheric $CO_2$ caused by changes in citizens' habits, either related or not to COVID-induced restrictions, the amount of the emitted $CO_2$ from the urban area can be evaluated by analyzing the temporal evolution in EC measurements. As shown in Fig. 3B, where the temporal variation of urban $CO_2$ fluxes measured in Florence before, during and after the confinement time is reported in terms of both (i) daily averages (black dashed curve) and (ii) 15-day rolling averages (red curve), daily $CO_2$ flux averages were characterized by a wide day-by-day variability. However, a clear stepwise decreasing trend was recognized, with three distinct time intervals of nearly steady-state conditions being separated by abrupt and sudden shifts and roughly corresponding to *PRE*, *LH* and *LN* phases. In particular, the temporal evolution in urban $CO_2$ fluxes at the beginning of the lockdown period (from *PRE* to *LH* phases) resembled that of road mobility (Fig. 2A), with a ca. 60% reduction coincident with the entry into force of the *#Iorestoacasa* decree law (Fig. 3B). The transition from *PRE* to *LH* phases was characterized by changes in the diurnal cycle of $CO_2$ fluxes (Fig. 4A), as follows: (i) overall reduction of ca. 23 μmol $m^{-2}$ $s^{-1}$ on average (corresponding to a drop of ca. 62% with respect to *PRE* levels), increasing at 30 and 36 μmol $m^{-2}$ $s^{-1}$ during the morning (8:00–11:00) and evening (20:00–23:00) peaks, respectively (corresponding to a reduction of 48 and 78%, respectively), and (ii) disappearance of the evening peak in the diurnal cycle of $CO_2$ fluxes during the *LH* phase, mostly related to the reduction in urban road traffic. Hence, the $CO_2$ fluxes during the *LH* phase (oscillating around 13 μmol $m^{-2}$ $s^{-1}$), being mainly governed by domestic heating, provided a rough estimation of $CO_2$ emissions from housing at the end of the heating season. Not surprisingly, the *LN* phase, i.e. when the vehicular traffic was stopped, was characterized by (i) an overall decrease of ca. 10 μmol $m^{-2}$ $s^{-1}$ in daily-averaged $CO_2$ fluxes with respect to *LH* phase (Fig. 3B), and (ii) the disappearance of the morning peak in $CO_2$ fluxes (Fig. 4B), with a drop of ca. 27 μmol $m^{-2}$ $s^{-1}$ in the 8:00–11:00 time interval.

Lastly, no significant differences were observed in the $CO_2$ fluxes between *LN* and *P2* phases, although the more constant diurnal pattern observed during the *P2* phase (Fig. 4B) is likely testifying the resumption of traffic as a major driver of $CO_2$ fluxes from the urban area during the non-heating season. A slight increase in the $CO_2$ fluxes was indeed observed after the beginning of phase 2, with an increase in daily-averaged EC fluxes of ca. 0.06 μmol $m^{-2}$ $s^{-1}$ per day.

### 4.4. Temporal variations in urban $CO_2$ concentrations

The observed temporal patterns in urban $CO_2$ fluxes evidenced a rapid response of EC measurements to changes in the urban sources of GHG caused by COVID-related measures and domestic heating switch-off, testified by the variations in $\delta^{13}C$-$CO_2$ values. Similarly, despite the small variations in concentrations and carbon isotopic values of $CH_4$ throughout the observation period (<0.1 ppm and around 1‰ vs. V-PDB; Fig. 5), the progressively increasing trend in the $\delta^{13}C$-$CH_4$ values confirmed the decrease in GHG contribution from natural gas consumption during the *LN* and *P2* phases. On the other hand, the impact of such changes on urban atmospheric $CO_2$ concentrations should not be considered so obvious. In fact, differently from short-term pollutants, $CO_2$ persists in the atmosphere for long time, progressively accumulating in a continuously increasing trend. As a consequence, despite the cutting in $CO_2$ emissions due to the COVID-19 crisis (Le Quéré et al., 2020), a negligible effect was observed on the buildup of global atmospheric $CO_2$ levels (Betts et al., 2020), a phenomenon that was effectively depicted with the renowned imagery of a filling bathtub: the water inflow through the tub represents $CO_2$ emissions, whereas the water level corresponds to the $CO_2$ concentration in the atmosphere, which is the actual responsible for long-term climate change; hence,

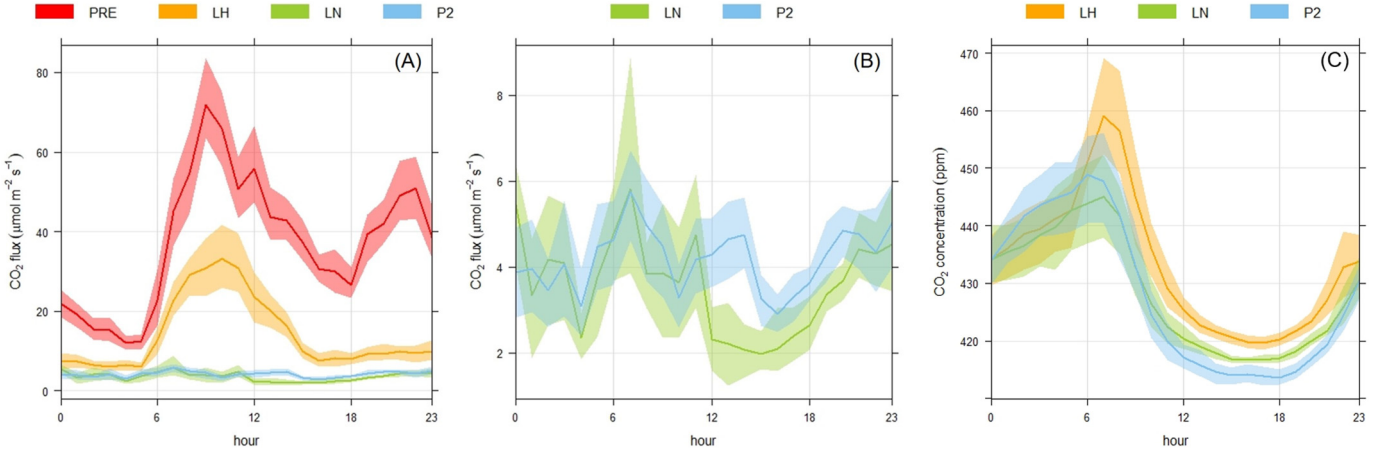


**Fig. 4.** (A) Diurnal cycle of $CO_2$ fluxes (in μmol $m^{-2}$ $s^{-1}$) during *PRE* (red curve), *LH* (orange curve), *LN* (yellow curve) and *P2* (cyan curve) phases. In (B), a focus on diurnal pattern of $CO_2$ fluxes during *LN* and *P2* phases is reported. In (C), diurnal cycle of $CO_2$ concentrations (in ppm) measured at DST-Unifi during *LH* (orange curve), *LN* (yellow curve) and *P2* (cyan curve) phases is shown. The shaded areas represent 95% confidence intervals.

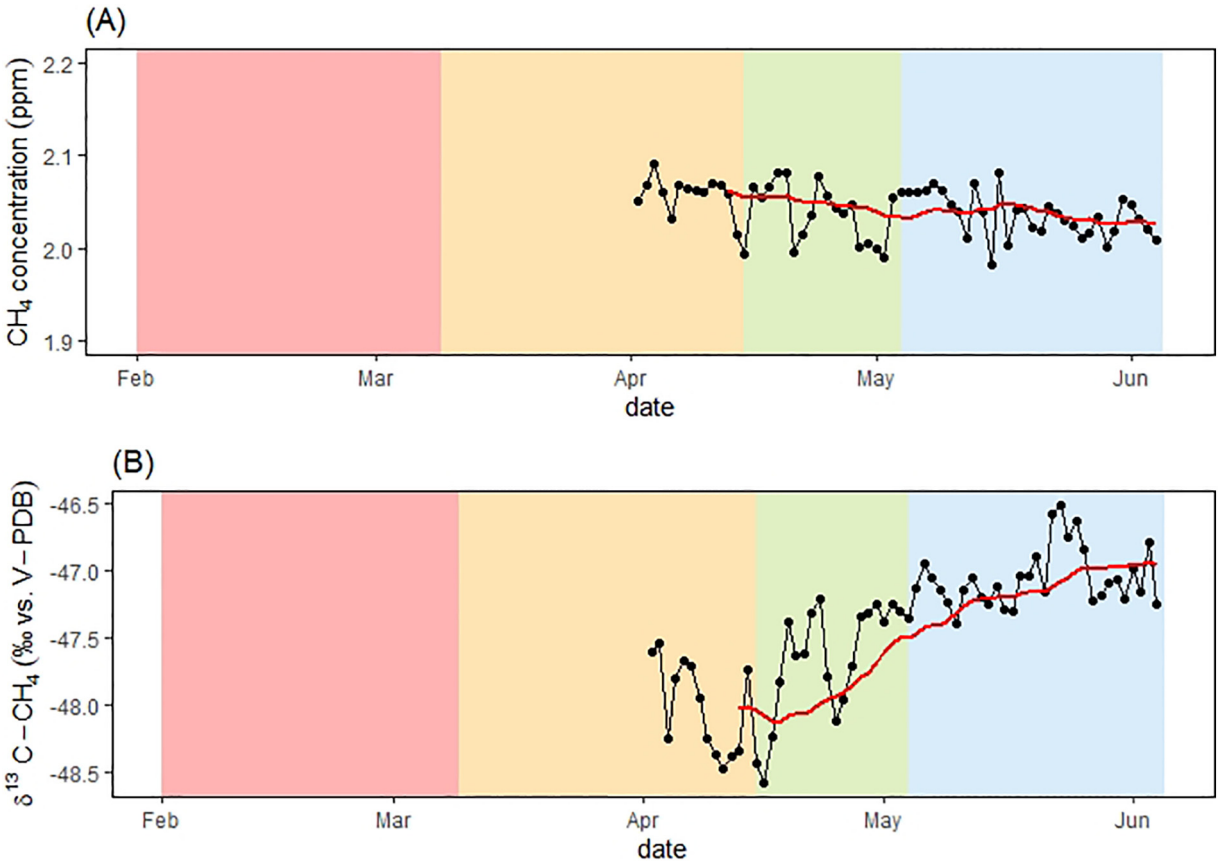


**Fig. 5.** Temporal pattern of (A) $CH_4$ concentrations and (B) $\delta^{13}C$-$CH_4$ values, expressed as daily averages (black dashed curve) and 15-day rolling averages (red curve). The colored areas refer to *PRE* (red), *LH* (orange), *LN* (yellow) and *P2* (cyan) phases.

even if the emissions are reduced, the bathtub continue to fill although at a slower rate (Sterman and Sweeney, 2007; Sterman, 2011).

The temporal variation of daily $CO_2$ concentration averages measured at street level is shown in Fig. 3B, where it is compared with both EC measurements and daily $CO_2$ concentration averages registered by the EC station. Similarly to $CO_2$ fluxes, daily $CO_2$ concentration averages were characterized by large day-by-day fluctuations. However, the 15-day rolling averages highlighted an overall decrease in diurnal $CO_2$ concentrations during the whole monitoring period (Fig. 3B). While data from EC station revealed strong decreases in $CO_2$ concentrations at the transition from *PRE* to *LH* phase and at the end of the heating season, $CO_2$ levels from April to June showed minor variations at both roof and street level. The diurnal $CO_2$ concentrations measured at street level were higher than those recorded at the rooftop of the Ximenes observatory, likely due to a vertical stratification and a buildup effect of atmospheric $CO_2$ concentrations within the urban street canyons. Noteworthy, a steeper decrease in diurnal $CO_2$ concentrations measured at street level was recognized during the *LN* phase after the end of the heating season. However, differently from EC flux data, daily $CO_2$ concentration averages did not show a clear stepwise trend with shifts concomitant with changes in the urban emitting patterns. Similarly, no relevant variations were observed in the diurnal cycle of $CO_2$ concentrations (Fig. 4C), which were characterized by a peak around 06–08 and lowest values during afternoon. The morning peak appeared to be more pronounced during the *LH* phase and more flattened during the *LN* phase.

However, it must be taken into account that measured $CO_2$ concentrations are the results of mixing between background levels and contributions from emitting sources, with varying quantitative ratios as a function of (i) variability of atmospheric turbulence, (ii) seasonal changes in background concentrations and (iii) variations in the strength of the emitting sources. Although the use of 15-day rolling averages limited the influence of the first factor, the decreasing trend observed in daily $CO_2$ concentration averages could still be affected by both seasonality, leading to a decrease in background $CO_2$ levels in spring and summer in the Northern Hemisphere, and changes in local $CO_2$ emissions. In order to distinguish these different effects, a statistical analysis of the $CO_2$ concentration data was performed. The frequency distribution of data was investigated using histograms. As an example, the histograms produced considering one-second-frequent $CO_2$ concentrations of the whole dataset and of *LH*, *LN* and *P2* phases are shown in Fig. 6A–D, although similar histograms were constructed for each day (not shown). The analysis of the histograms revealed that $CO_2$ concentrations were described by the mixing of two distinct normal populations. The first one (hereafter, population *A*) was centered around 419 ppm and described the 60% of the whole dataset. The second one (hereafter, population *B*) was centered around 445 ppm and represented the remaining 40% of the data. This indicates two alternative states of the atmospheric $CO_2$ levels, which roughly corresponded to (i) afternoon and (ii) early morning rush hour (5:00–9:00) conditions (Fig. 4C), i.e. related to (i) high convective turbulence conditions promoting dispersion and dilution phenomena and (ii) more stable conditions favoring buildup of airborne contaminants, respectively. The temporal variation of the barycenter of the two populations, expressed as 15-day rolling average, is shown in Fig. 6E. Population *A* displayed a nearly constant decreasing trend, with a slope of ca. −0.14 ppm/day, mostly related to seasonal fluctuations of the background $CO_2$ levels and seasonal variability of atmospheric turbulence dynamics. Differently, population *B* was characterized by a less regular pattern, with an overall decreasing trend interrupted by a trough during the *LN* phase. In order to decompose the temporal trend of population *A* and remove the effect of seasonality, the difference between populations *B*

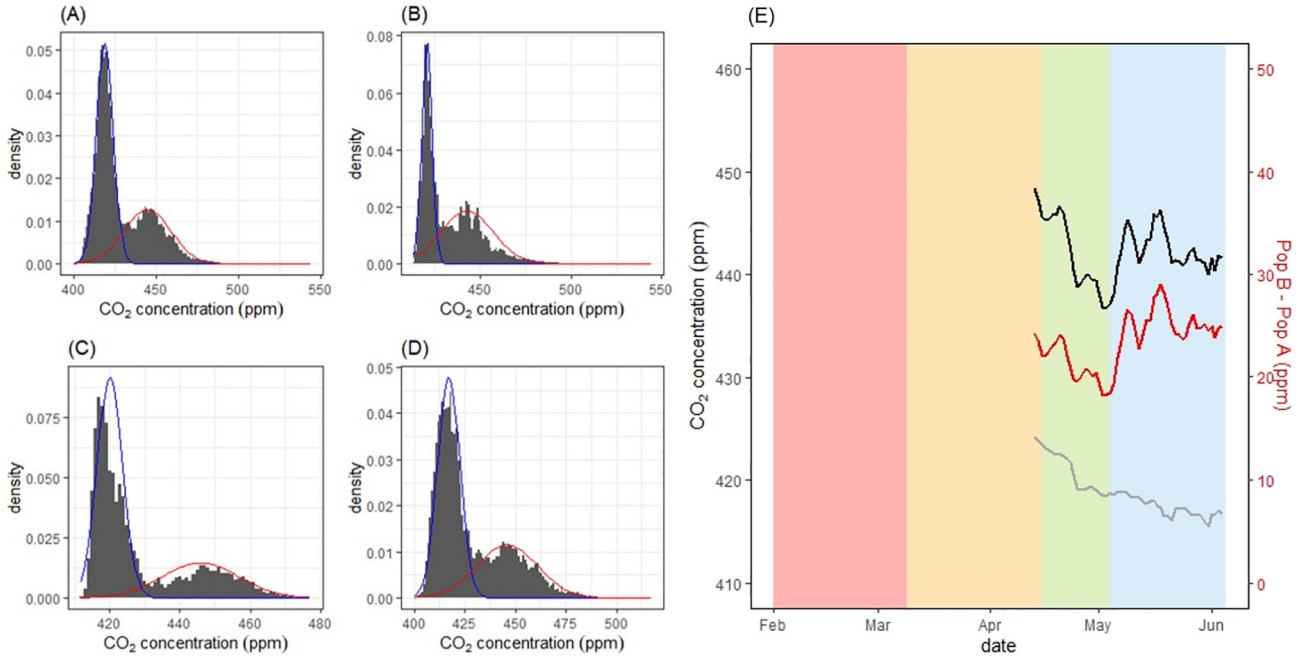


**Fig. 6.** Density distribution diagram of one-second-frequent $CO_2$ concentrations (in ppm) of (A) the whole dataset, (B) *LH*, (C) *LN* and (D) *P2* phases. Blue and red curves depict population *A* and *B*, respectively, as described in the text. (E) Temporal pattern of mean $CO_2$ concentrations (in ppm), expressed as 15-day rolling averages, obtained for populations *A* (grey curve) and *B* (black curve), as described in the text. The difference between the two populations is also reported (red curve). The colored areas refer to *PRE* (red), *LH* (orange), *LN* (yellow) and *P2* (cyan) phases.

and *A* was calculated (Fig. 6E). The obtained values corresponded to the daily $CO_2$ enhancement not related to fluctuations in background values and dispersion dynamics but more strictly governed by the strength of local emitting sources, which are expected to directly influence the peak-to-trough amplitude of the diurnal $CO_2$ variations (Fig. 4C). As evidenced in Fig. 6E, $CO_2$ concentrations experienced a progressive decrease throughout *LN* phase, followed by a net increase at the beginning of *P2* phase with a shift of ca. 5 ppm from the beginning to the half of May, when a stabilization in the difference between populations *A* and *B* was observed, resembling both the temporal pattern of urban road mobility (Fig. 2A) and the evolution of the isotopic signature of non-background atmospheric $CO_2$ (Fig. 3A), and hence representing the contribution from the resumption of urban traffic.

### 4.5. Distributional analysis and structure of the system dynamics

The distributional analysis of the concentrations of $CO_2$ (ppm) measured by the Picarro G2201-i cavity ring-down spectrometer (CRDS) and the $\delta^{13}C$-$CO_2$ are reported in Fig. 7A and B, respectively, following the idea of Scheffer et al. (2012) to reverse the y-axis, thus considering the probability density as a proxy of the effect of a potential related to the action of the environmental drivers. Kernel Density Estimation (KDE) was used as a non-parametric way to evaluate the shape of the probability density function of the analyzed random variables (Ahmad and Ran, 2004). The configuration allowed to identify the presence of different basins of attraction for data and, consequently, the flickering of the systems to different alternative states. The $CO_2$ concentration was exactly in the last situation, showing alternative states that can be populated by the data depending on the effect of external drivers (Fig. 7A); on the other hand, $\delta^{13}C$-$CO_2$ presented a more stable configuration (Fig. 7B). The statistical analysis of the time-behavior for $CO_2$ concentrations measured during the whole monitoring period indicated that the series was not stationary (KPSS test, $p < 0.05$, presence of a decreasing trend) and that the rankings of values were not random (*runs* test, $p < 0.05$; Kwiatkowski et al., 1992; Alhakim and Hooper, 2008). A similar result was obtained for the $\delta^{13}C$-$CO_2$ values but related to an increasing trend. These evidences agreed with previous observations based on an exploratory analysis of the dataset and highlighted the occurrence of a seasonal effect largely governing the overall temporal trend of $CO_2$ concentrations and isotopic composition. Consequently, in both the situations autocorrelation in time was expected, but the $\delta^{13}C$-$CO_2$ values appeared to have a higher capacity of recovery under perturbation with respect to the $CO_2$ concentration, due to the absence of different attraction basins able to generate flickering. This condition also had an important effect on data variance in time. Thus, both the variables showed a gradual change in time but more instability was expected for $CO_2$ when compared to the $\delta^{13}C$-$CO_2$ data with respect to the variation in environmental drivers. Accordingly, the partitioning of data into *LH*, *LN* and *P2* phases did not produce a significant change in the shape of $\delta^{13}C$-$CO_2$ configuration, except for a shift towards higher values as a consequence of the seasonal trend (Fig. 7B). Differently, in the case of $CO_2$ concentrations (Fig. 7A), the COVID-19 lockdown period (*LH* and *LN* phases) did not result in a change of the overall data distribution, but it produced an evident deepening of the first basin of attraction, corresponding to low $CO_2$ levels. Noteworthy, both $CO_2$ and $\delta^{13}C$-$CO_2$ variables tended to follow a Gaussian distribution (or a mixture between two Gaussian distributions) for which variability around the mean emerges from the combined, additive influence of innumerable weak, accidental and mutually independent factors. Accordingly, while the confinement measures directly affected atmospheric $CO_2$ concentrations, in line with previous observations, removing part of active $CO_2$ sources, they did not change the overall frequency distribution shape of data, which was largely governed by natural environmental components. These results were in line with findings by Gualtieri et al. (2021) who evidenced that emission reduction actions alone have limited effects on $CO_2$ concentrations at local urban scale due to the large influence played by meteorological conditions. Nevertheless, the deepening of the first basin of attraction (Fig. 7A) testified that the COVID-19 restrictions made low $CO_2$ concentrations more resilient, that is more resistant to perturbations in time until a new threshold is achieved. Consequently, it is reliable to affirm that the changes of citizen habits during the pandemic produced a

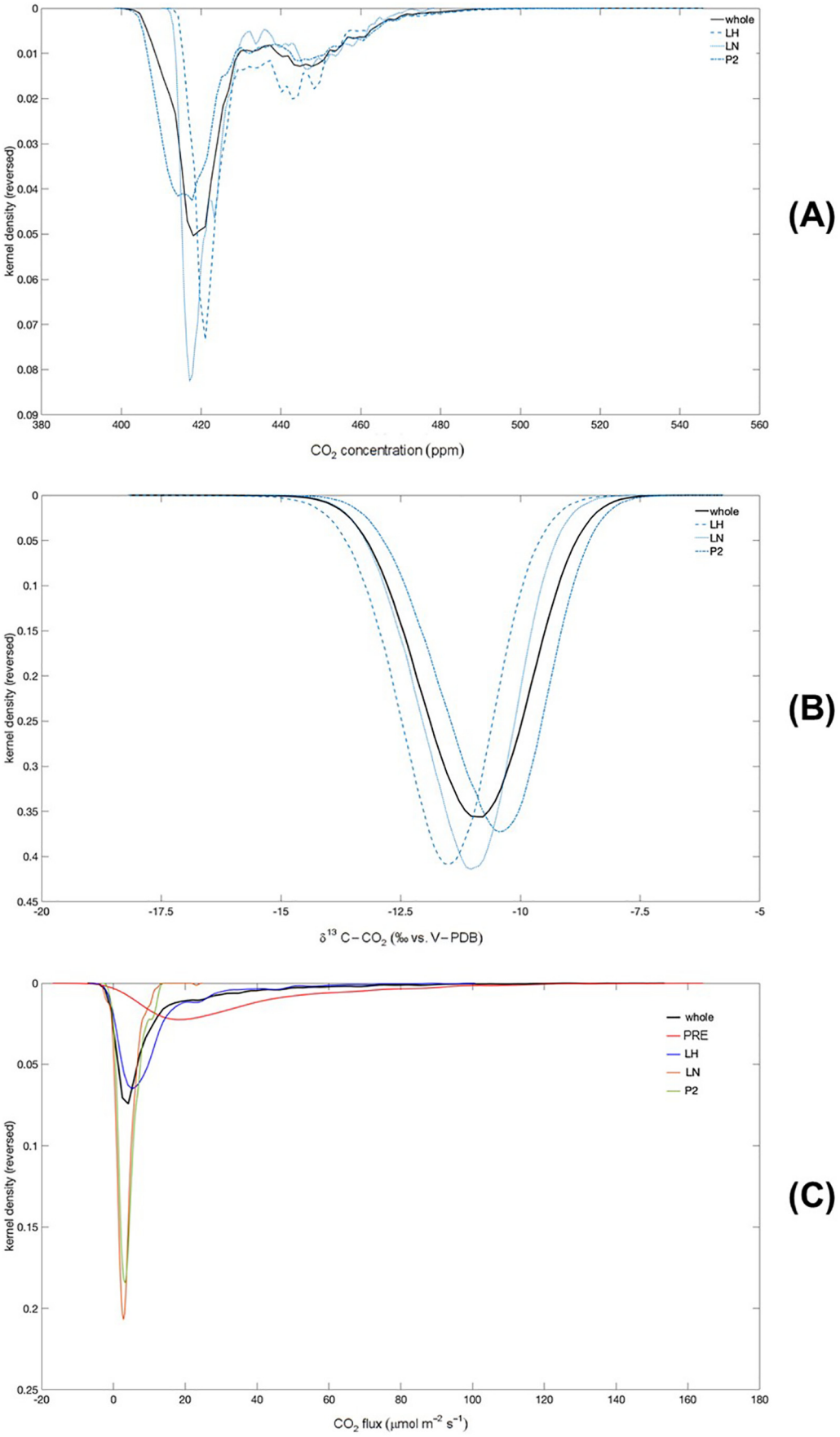


**Fig. 7.** Probability density distribution (with reversed y-axis) of (A) $CO_2$ concentrations (in ppm), (B) $\delta^{13}C$-$CO_2$ and (C) $CO_2$ fluxes (in μmol $m^{-2}$ $s^{-1}$) are reported for the whole observation period and for *PRE*, *LH*, *LN* and *P2* phases.

tangible, though limited, effect on urban atmospheric $CO_2$ levels with high values becoming less frequent. In particular, the second basin of attraction, i.e. that corresponding to relatively high $CO_2$ levels, appeared to be highly unstable and largely depending on the strength of the emission sources. Accordingly, the consistency of the frequency distribution shape for the $\delta^{13}C$-$CO_2$ values during *LH*, *LN* and *P2* phases confirmed that, independently from the characteristics of the emission processes, atmospheric $CO_2$ dynamics at urban scale were strictly controlled by dilutive effects regulated by source strengths and turbulent atmospheric diffusion and transport. The discrepancy of behavior between $CO_2$ and $\delta^{13}C$-$CO_2$ has important implications in correlating (e.g. binary plots) the two variables for interpret geochemical processes since for the first one the variance could have an important role in masking plurimodality (alternative states) not corresponding in the second one.

The analysis of the frequency distribution shape for the $CO_2$ fluxes measured during the whole observation period (Fig. 7C) allows us to visualize a further situation characterized by an asymmetrical frequency distribution where high values are a rarer event. The whole distribution could follow an exponential model (normal, log-normal and power law models being more distant) as the expression of additive perturbations in time supporting the hypothesis that component processes themselves, instead of interactions among systems' components, dominate the observed variability (van Rooij et al., 2013). The runs and KPSS test indicate that also the $CO_2$ flux time series is not stationary and random so that autocorrelation is expected, in agreement with the decreasing trend evidenced in Fig. 3B. The partitioning of data into *PRE*, *LH*, *LN* and *P2* phases highlighted a change in the frequency distribution shape for the $CO_2$ fluxes (Fig. 7C). While the *PRE* phase displayed a flattened curve with a large fraction of high $CO_2$ flux values, the onset of the lockdown resulted in the occurrence of a basin of attraction at low $CO_2$ flux values. While the *LH* phase preserved a significant fraction of high $CO_2$ flux values, as a consequence of domestic heating, the *LN* phase displayed an abrupt deepening of the basin of attraction, which was only partially recovered during *P2* phase, and that represented the amount of $CO_2$ emissions related to urban basal metabolism.

Summarizing, in all the analyzed cases the variables describe a component-dominant dynamics. Interactions and feedback mechanisms thus appear to be minimized. In the case of $CO_2$ concentrations and $\delta^{13}C$-$CO_2$ values the dynamics appears to preserve information only about the mean and the variance while in the case of $CO_2$ flux measurements, basically exponential (a continuous distribution that has highest probability for zero or small values), only information about the mean is preserved (Frank, 2009).

In this framework, the COVID-19 restrictions appear to have had a peculiar impact on the $CO_2$ concentration measures, thus enhancing the presence of stable alternative states, even if in a restricted time interval, permitting the flickering of the system.

## 5. Conclusions

The present study has demonstrated that the dramatic drop in human activities produced appreciable reductions in $CO_2$ fluxes and in atmospheric $CO_2$ concentrations (in terms of local $CO_2$ enhancement) and related carbon isotopic signature measured at urban scale, evidencing the impact of COVID-related restrictions on the urban $CO_2$ plume. In particular, EC $CO_2$ fluxes showed a rapid response to changes in the strength of urban emitting sources, with fast and abrupt transitions between different steady-state conditions before the national lockdown period, at the end of the heating season and during the progressive resumption of normal urban functions and citizens' habits, with variations in the magnitude of $CO_2$ fluxes being related to the extent of $CO_2$ emissions from the main urban GHG sources, i.e. natural gas consumption and vehicular traffic. Accordingly, the stop imposed to urban mobility caused a ca. 62% reduction of urban $CO_2$ fluxes, corresponding to a decrease of 23 μmol $m^{-2}$ $s^{-1}$, which approximates the contribution from local vehicular traffic. On the other hand, the end of the heating season caused a drop up to 27 μmol $m^{-2}$ $s^{-1}$ during the morning peak of the diurnal pattern of urban $CO_2$ fluxes associated to the consumption of natural gas for the warming up of the buildings.

Similarly, the temporal evolution in the isotopic signature of atmospheric $CO_2$ confirmed the direct impact of the changing GHGs sources on the $CO_2$ buildup in the urban air. Accordingly, although the daily-averaged $CO_2$ concentrations showed no remarkable variations clearly attributable to COVID-related restrictions at first sight, an in-depth analysis on the diurnal cycle of $CO_2$ concentrations allowed to recognize the direct footprint of the easing in urban mobility restrictions on the diurnal $CO_2$ enhancement.

Results on the shape of frequency distribution confirmed that some essential features of the dynamics that govern stochastic environmental systems can be understood without specific knowledge about the components affecting the system itself (Holden et al., 2009; Holden and Rajaraman, 2012). The obtained indications could be instead used to formulate hypothesis to build-up basic generative models for further developments. In our case, it emerges the role played by the variance that could be used in future as an early warning signals to monitor changes in time. It is, indeed, a statistic whose behavior is able to move data from one distribution to another, governing the passage among different distributions (log-normal, power laws or exponential models), and contributing to the presence of stable/instable alternative states (Mitzenmacher, 2004; Scheffer et al., 2012; van Rooij et al., 2013).

Unveiling the relationships between human activities, $CO_2$ emissions and atmospheric $CO_2$ concentrations at urban scale through appropriate GHGs monitoring networks will be important to develop adequate emission accounting and verification methodologies, helping to build the sustainable cities of the next future, on the front line in the fight against climate change, and guiding the local, national and supranational political strategies.

## CRediT authorship contribution statement

**Stefania Venturi:** Conceptualization, Methodology, Software, Formal analysis, Writing – original draft, Visualization, Project administration. **Antonio Randazzo:** Conceptualization, Writing – original draft, Visualization. **Franco Tassi:** Conceptualization, Writing – review & editing, Supervision, Project administration. **Beniamino Gioli:** Conceptualization, Data curation, Validation, Writing – review & editing, Project administration. **Antonella Buccianti:** Conceptualization, Methodology, Software, Formal analysis, Writing – original draft, Visualization. **Giovanni Gualtieri:** Investigation, Data curation, Writing – review & editing. **Francesco Capecchiacci:** Investigation, Resources, Data curation. **Jacopo Cabassi:** Investigation, Data curation, Writing – review & editing. **Lorenzo Brilli:** Investigation, Resources, Data curation, Writing – review & editing. **Federico Carotenuto:** Investigation, Data curation, Writing – review & editing. **Riccardo Santi:** Investigation, Data curation. **Carolina Vagnoli:** Investigation, Resources, Data curation. **Alessandro Zaldei:** Investigation, Data curation, Writing – review & editing. **Orlando Vaselli:** Supervision, Writing – review & editing.

## Declaration of competing interest

The authors declare that they have no known competing financial interests or personal relationships that could have appeared to influence the work reported in this paper.

## Acknowledgments

The authors want to thank the Ximenes Observatory foundation for the logistical support and Estra Ltd. for having shared data on natural gas consumption.

## References


Abdullah, S., Mansor, A.A., Napi, N.N.L.M., Nurdiyana, W., Mansor, W., Ahmed, A.N., Ismail, M., Ramly, Z.T.A., 2020. Air quality status during 2020 Malaysia Movement Control Order (MCO) due to 2019 novel coronavirus (2019-nCoV) pandemic. Sci. Total Environ. 729, 139022. https://doi.org/10.1016/j.scitotenv.2020.139022.

Adams, M.D., 2020. Air pollution in Ontario, Canada during the COVID-19 state of emergency. Sci. Total Environ. 742, 140516. https://doi.org/10.1016/j.scitotenv.2020.140516.

Ahmad, I.A., Ran, I.S., 2004. Data based bandwidth selection in kernel density estimation with parametric start via kernel contrasts. J. Nonparametric Stat. 16 (6), 841–877. https://doi.org/10.1080/10485250310001652601.

Alhakim, A., Hooper, W., 2008. A non-parametric test for several independent samples. J. Nonparametric Stat. 20 (3), 253–261. https://doi.org/10.1080/10485250801976741.

Aubinet, M., Grelle, A., Ibrom, A., Rannik, Ü., Moncrieff, J., Foken, T., Kowalski, A.S., Martin, P.H., Berbigier, P., Bernhofer, Ch., Clement, R., Elbers, J., Granier, A., Grünwald, T., Morgenstern, K., Pilegaard, K., Rebmann, C., Snijders, W., Valentini, R., Vesala, T., 2000. Estimates of the annual net carbon and water exchange of forests: the EUROFLUX methodology. Adv. Ecol. Res. 30, 113–175. https://doi.org/10.1016/S0065-2504(08)60018-5.

Baldasano, J.M., 2020. COVID-19 lockdown effects on air quality by $NO_2$ in the cities of Barcelona and Madrid (Spain). Sci. Total Environ. 741, 140353. https://doi.org/10.1016/j.scitotenv.2020.140353.

Baur, A.H., Thess, M., Kleinschmit, B., Creutzig, F., 2014. Urban climate change mitigation in Europe: looking at and beyond the role of population density. J. Urban Plan. Develop. 140 (1), 04013003. https://doi.org/10.1061/(ASCE)UP.1943-5444.0000165.

Bauwens, M., Compernolle, S., Stavrakou, T., Müller, J.F., van Gent, J., Eskes, H., Levelt, P.F., van der, A.R., Veefkind, J.P., Vlietinck, J., Yu, H., Zehner, C., 2020. Impact of coronavirus outbreak on $NO_2$ pollution assessed using TROPOMI and OMI observations. Geophys. Res. Lett. 47. https://doi.org/10.1029/2020GL087978 e2020GL087978.

Berman, J.D., Ebisu, K., 2020. Changes in U.S. air pollution during the COVID-19 pandemic. Sci. Total Environ. 739, 139864. https://doi.org/10.1016/j.scitotenv.2020.139864.

Betts, R., Jones, C., Jin, Y., Kelling, R., Kennedy, J., Knight, J., Scaife, A., 2020. Analysis: what impact will the coronavirus pandemic have on atmospheric $CO_2$? https://www.carbonbrief.org/analysis-what-impact-will-the-coronavirus-pandemic-have-on-atmospheric-co2. (Accessed 30 December 2020)

Brauner, J.M., Mindermann, S., Sharma, M., Johnston, D., Salvatier, J., Gavenciak, T., Stephenson, A.B., Leech, G., Altman, G., Mikulik, V., Norman, A.J., Monrad, J.T., Besiroglu, T., Ge, H., Hartwick, M.A., The, Y.W., Chindelevitch, L., Gal1, Y., Kulveit, J., 2020. Inferring the effectiveness of government interventions against COVID-19. Science, eabd9338 https://doi.org/10.1126/science.abd9338.

Carslaw, D.C., 2014. The Openair Manual — Open-Source Tools for Analyzing Air Pollution Data Manual for version 1.0, King's College London.

Carslaw, D.C., Ropkins, K., 2012. openair — an R package for air quality data analysis. Environ. Model Softw. 27-28, 52–61. https://doi.org/10.1016/j.envsoft.2011.09.008.

Chamberlain, S.D., Ingraffea, A.R., Sparks, J.P., 2016. Sourcing methane and carbon dioxide emissions from a small city: influence of natural gas leakage and combustion. Environ. Pollut. 218, 102–111. https://doi.org/10.1016/j.envpol.2016.08.036.

Clark-Thorne, S.T., Yapp, C.J., 2003. Stable carbon isotope constraints on mixing and mass balance of $CO_2$ in an urban atmosphere: Dallas metropolitan area, Texas, USA. Appl. Geochem. 18, 75–95. https://doi.org/10.1016/S0883-2927(02)00054-9.

Collivignarelli, M.C., Abbà, A., Bertanza, G., Pedrazzani, R., Ricciardi, P., Carnevale Miino, M., 2020. Lockdown for CoViD-2019 in Milan: what are the effects on air quality? Sci. Total Environ. 732, 139280. https://doi.org/10.1016/j.scitotenv.2020.139280.

Dantas, G., Siciliano, B., França, B.B., da Silva, C.M., Arbilla, G., 2020. The impact of COVID-19 partial lockdown on the air quality of the city of Rio de Janeiro, Brazil. Sci. Total Environ. 729, 139085. https://doi.org/10.1016/j.scitotenv.2020.139085.

Decree of the President of the Republic (DPR) no. 412 of 26/08/1993. Regulations on design, installation, operation and maintenance of building heating systems for limiting energy consumption. Official Gazette no. 242, 14/10/1993.

Duren, R.M., Miller, C.E., 2012. Measuring the carbon emissions of megacities. Nat. Clim. Chang. 2 (8), 560–562.

Elsaid, K., Olabi, V., Sayed, E.T., Wilberforce, T., Abdelkareem, M.A., 2021. Effects of COVID-19 on the environment: an overview on air, water, wastewater, and solid waste. J. Environ. Manag. 292, 112694. https://doi.org/10.1016/j.jenvman.2021.112694.

EnelX & Here, 2020. City Analytics e Mobility Map. https://enelxmobilityflowanalysis.here.com/dashboard/ITA/info.html.

Foken, T., Wichura, B., 1996. Tools for quality assessment of surface-based flux measurements. Agric. For. Meteorol. 78 (1–2), 83–105. https://doi.org/10.1016/0168-1923(95)02248-1.

Frank, S., 2009. The common patterns of nature. J. Evol. Biol. 22 (8), 1563–1585. https://doi.org/10.1111/j.1420-9101.2009.01775.x.

Gioli, B., Toscano, P., Lugato, E., Matese, A., Miglietta, F., Zaldei, A., Vaccari, F.P., 2012. Methane and carbon dioxide fluxes and source partitioning in urban areas: the case study of Florence, Italy. Environ. Pollut. 164, 125–131. https://doi.org/10.1016/j.envpol.2012.01.019.

Gioli, B., Gualtieri, G., Busillo, C., Calastrini, F., Zaldei, A., Toscano, P., 2015. Improving high resolution emission inventories with local proxies and urban eddy covariance flux measurements. Atmos. Environ. 115, 246–256. https://doi.org/10.1016/j.atmosenv.2015.05.068.

Górka, M., Lewicka-Szczebak, D., 2013. One-year spatial and temporal monitoring of concentration and carbon isotopic composition of atmospheric $CO_2$ in a Wrocław (SW Poland) city area. Appl. Geochem. 35, 7–13. https://doi.org/10.1016/j.apgeochem.2013.05.010.

Gualtieri, G., Brilli, L., Carotenuto, F., Vagnoli, C., Zaldei, A., Gioli, B., 2020. Quantifying road traffic impact on air quality in urban areas: a Covid19-induced lockdown analysis in Italy. Environ. Pollut. 267, 115682. https://doi.org/10.1016/j.envpol.2020.115682.

Gualtieri, G., Di Lonardo, S., Carotenuto, F., Toscano, P., Vagnoli, C., Zaldei, A., Gioli, B., 2021. The role of emissions and meteorology in driving $CO_2$ concentrations in urban areas. Environ. Sci. Pollut. Res. https://doi.org/10.1007/s11356-021-12754-8.

Han, P., Cai, Q., Oda, T., Zeng, N., Shan, Y., Lin, X., Lin, D., 2021. Assessing the recent impact of COVID-19 on carbon emissions from China using domestic economic data. Sci. Total Environ. 750, 141688. https://doi.org/10.1016/j.scitotenv.2020.141688.

Haug, N., Geyrhofer, L., Londei, A., Dervic, E., Desvars-Larrive, A., Loreto, V., Pinior, B., Thurner, S., Klimek, P., 2020. Ranking the effectiveness of worldwide COVID-19 government interventions. Nat. Hum. Behav. 4, 1303–1312. https://doi.org/10.1038/s41562-020-01009-0.

Holden, J.G., Rajaraman, S., 2012. The self-organization of a spoken word. Front. Psychol. 3, 209. https://doi.org/10.3389/fpsyg.2012.00209.

Holden, J.G., Van Orden, G.C., Turvey, M.Y., 2009. Dispersion of response times reveals cognitive dynamics. Pshychol. Rev. 116, 318–342. https://doi.org/10.1037/a0014849.

Hoornweg, D., Sugar, L., Lorena, C., Gómez, T., 2011. Cities and greenhouse gas emissions: moving forward. Environ. Urban. 23 (1), 207–227. https://doi.org/10.1177/0956247810392270.

Hutyra, L.R., Duren, R., Gurney, K.R., Grimm, N., Kort, E.A., Larson, E., Shrestha, G., 2014. Urbanization and the carbon cycle: current capabilities and research outlook from the natural sciences perspective. Earth's Future 2, 473–495. https://doi.org/10.1002/2014EF000255.

IPCC, 2018. Global warming of 1.5 °C. An IPCC special report on the impacts of global warming of 1.5 °C above pre-industrial levels and related global greenhouse gas emission pathways, in the context of strengthening the global response to the threat of climate change, sustainable development, and efforts to eradicate poverty. In: Masson-Delmotte, V., Zhai, P., Pörtner, H.-O., Roberts, D., Skea, J., Shukla, P.R., Pirani, A., Moufouma-Okia, W., Péan, C., Pidcock, R., Connors, S., Matthews, J.B.R., Chen, Y., Zhou, X., Gomis, M.I., Lonnoy, E., Maycock, T., Tignor, M., Waterfield, T. (Eds.), 2019 Intergovernmental Panel on Climate Change, p. 616.

Keeling, C.D., 1958. The concentration and isotopic abundances of atmospheric carbon dioxide in rural areas. Geochim. Cosmochim. Acta 13, 322–334. https://doi.org/10.1016/0016-7037(58)90033-4.

Keeling, C.D., 1961. The concentration and isotopic abundances of carbon dioxide in rural and marine air. Geochim. Cosmochim. Acta 24, 277–298. https://doi.org/10.1016/0016-7037(61)90023-0.

Keeling, C.D., Piper, S.C., Bacastow, R.B., Wahlen, M., Whorf, T.P., Heimann, M., Meijer, H.A., 2005. Atmospheric $CO_2$ and $^{13}CO_2$ exchange with the terrestrial biosphere and oceans from 1978 to 2000: observations and carbon cycle implications. In: Ehleringer, J.R., Cerling, T.E., Dearing, M.D. (Eds.), A History of Atmospheric $CO_2$ and Its Effects on Plants, Animals, and Ecosystems. 2005. Springer Verlag, New York, pp. 83–113.

Kerimray, A., Baimatova, N., Ibragimova, O.P., Bukenov, B., Kenessov, B., Plotitsyn, P., Karaca, F., 2020. Assessing air quality changes in large cities during COVID-19 lockdowns: the impacts of traffic-free urban conditions in Almaty, Kazakhstan. Sci. Total Environ. 730, 139179. https://doi.org/10.1016/j.scitotenv.2020.139179.

Khan, I., Shah, D., Shah, S.S., 2020. COVID-19 pandemic and its positive impacts on environment: an updated review. Int. J. Environ. Sci. Technol. https://doi.org/10.1007/s13762-020-03021-3.

Kwiatkowski, D., Phillips, P.C.B., Schmidt, P., Shin, Y., 1992. Testing the null hypothesis of stationarity against the alternative of a unit root. J. Econ. 54, 159–178. https://doi.org/10.1016/0304-4076(92)90104-Y.

Le Quéré, C., Jackson, R.B., Jones, M.W., Smith, A.J., Abernethy, S., Andrew, R.M., De-Gol, A.J., Willis, D.R., Shan, Y., Canadell, J.G., Friedlingstein, P., Creutzig, F., Peters, G.P., 2020. Temporary reduction in daily global $CO_2$ emissions during the COVID-19 forced confinement. Nat. Clim. Chang. https://doi.org/10.1038/s41558-020-0797-x.

Li, L., Li, Q., Huanga, L., Wanga, Q., Zhu, A., Xua, J., Liu, Z., Li, H., Shi, L., Li, R., Azari, M., Wang, Y., Zhang, X., Liu, Z., Zhu, Y., Zhang, K., Xue, S., Ooi, M.C.G., Zhanga, D., Chan, A., 2020. Air quality changes during the COVID-19 lockdown over the Yangtze River Delta Region: an insight into the impact of human activity pattern changes on air pollution variation. Sci. Total Environ. 732, 139282. https://doi.org/10.1016/j.scitotenv.2020.139282.

Liu, Z., Ciais, P., Deng, Z., Lei, R., Davis, S.J., Feng, S., Zheng, B., Cui, D., Dou, X., Zhu, B., Guo, R., Ke, P., Sun, T., Lu, C., He, P., Wang, Y., Yue, X., Wang, Y., Lei, Y., Zhou, H., Cai, Z., Wu, Y., Guo, R., Han, T., Xue, J., Boucher, O., Boucher, E., Chevallier, F., Tanaka, K., Wei, Y., Zhong, H., Kang, C., Zhang, N., Chen, B., Xi, F., Liu, M., Bréon, F.M., Lu, Y., Zhang, Q., Guan, D., Gong, P., Kammen, D.M., He, K., Schellnhuber, H.J., 2020. Near-real-time monitoring of global $CO_2$ emissions reveals the effects of the COVID-19 pandemic. Nat. Commun. 11, 6292. https://doi.org/10.1038/s41467-020-20254-5.

Liu, D., Sun, W., Zeng, N., Han, P., Yao, B., Liu, Z., Wang, P., Zheng, K., Mei, H., Cai, Q., 2021. Observed decreases in on-road $CO_2$ concentrations in Beijing during COVID-19. Atmos. Chem. Phys. 21, 4599–4614. https://doi.org/10.5194/acp-21-4599-2021.

Lozzi, G., Rodrigues, M., Marcucci, E., Teoh, T., Gatta, V., Pacelli, V., 2020. Research for TRAN Committee – COVID-19 and Urban Mobility: Impacts and Perspectives. European Parliament, Policy Department for Structural and Cohesion Policies, Brussels.

Mahato, S., Pal, S., Ghosh, K.G., 2020. Effect of lockdown amid COVID-19 pandemic on air quality of the megacity Delhi, India. Sci. Total Environ. 730, 139086. https://doi.org/10.1016/j.scitotenv.2020.139086.

Marcotullio, P.J., Hughes, S., Sarzynski, A., Pincetl, S., Peña, L.S., Romero-Lankao, P., Runfola, D., Seto, K.C., 2014. Urbanization and the carbon cycle: contributions from social science. Earth's Future 2, 496–514. https://doi.org/10.1002/2014EF000257.

Mitchell, L.E., Lin, J.C., Bowling, D.R., Pataki, D.E., Strong, C., Schauer, A.J., Bares, R., Bush, S.E., Stephens, B.B., Mendoza, D., Mallia, D., Holland, L., Gurney, K.R., Ehleringer, J.R., 2018. Long-term urban carbon dioxide observations reveal spatial and temporal dynamics related to urban characteristics and growth. PNAS 115, 2912–2917. https://doi.org/10.1073/pnas.1702393115.

Mitzenmacher, M., 2004. A brief history of generative models for power law and lognormal distributions. Internet Math. 1, 226–251. https://doi.org/10.1080/15427951.2004.10129088.

Otmani, A., Benchrif, A., Tahri, M., Bounakhla, M., Chakir, E.M., El Bouch, M., Krombi, M., 2020. Impact of Covid-19 lockdown on PM10, $SO_2$ and $NO_2$ concentrations in Salé City (Morocco). Sci. Total Environ. 735, 139541. https://doi.org/10.1016/j.scitotenv.2020.139541.

Paital, B., 2020. Nurture to nature via COVID-19, a self-regenerating environmental strategy of environment in global context. Sci. Total Environ. 729, 139088. https://doi.org/10.1016/j.scitotenv.2020.139088.

Pang, J., Wen, X., Sun, X., 2016. Mixing ratio and carbon isotopic composition investigation of atmospheric $CO_2$ in Beijing, China. Sci. Total Environ. 539, 322–330. https://doi.org/10.1016/j.scitotenv.2015.08.130.

Papale, D., Reichstein, M., Aubinet, M., Canfora, E., Bernhofer, C., Kutsch, W., Longdoz, B., Rambal, S., Valentini, R., Vesala, T., Yakir, D., 2006. Towards a standardized processing of net ecosystem exchange measured with eddy covariance technique: algorithms and uncertainty estimation. Biogeosciences 3, 571–583. https://doi.org/10.5194/bg-3-571-2006.

Papale, D., Antoniella, G., Nicolini, G., Gioli, B., Zaldei, A., Vogt, R., Felgenwinter, C., Stagakis, S., Chrysoulakis, N., Järvi, L., Nemitz, E., Helfer, C., Barlow, J., Meier, F., Velasco, E., Christen, A., Masson, V., 2020. Clear evidence of reduction in urban $CO_2$ emissions as a result of COVID-19 lockdown across Europe. ICOS Report May 13, 2020. www.icos-ri.eu.

Pataki, D.E., Bowling, D.R., Ehleringer, J.R., 2003a. Seasonal cycle of carbon dioxide and its isotopic composition in an urban atmosphere: anthropogenic and biogenic effects. J. Geophys. Res. 108 (D23), 4735. https://doi.org/10.1029/2003JD003865.

Pataki, D.E., Ehleringer, J.R., Flanagan, L.B., Yakir, D., Bowling, D.R., Still, C.J., Buchmann, N., Kaplan, J.O., Berry, J.A., 2003b. The application and interpretation of Keeling plots in terrestrial carbon cycle research. Glob. Biogeochem. Cycles 17 (1), 1022. https://doi.org/10.1029/2001GB001850.

Pichler, P.P., Zwickel, T., Chavez, A., Kretschmer, T., Seddon, J., Weisz, H., 2017. Reducing urban greenhouse gas footprints. Sci. Rep. 7, 14659. https://doi.org/10.1038/s41598-017-15303-x.

R Core Team, 2017. R: A Language and Environment for Statistical Computing. https://www.R-project.org/.

Regione Toscana, 2010. Inventario regionale delle sorgenti di emissione in aria ambiente – IRSE. Aggiornamento all'anno 2010. Direzione Generale Politiche Territoriali Ambientali e per la Mobilità, Settore Energia, tutela della qualità dell'aria e dall'inquinamento elettromagnetico e acustico, Firenze, Italy.

van Rooij, M.M.J.W., Nash, B.A., Rajaraman, S., Holden, J.G., 2013. A fractal approach to dynamic inference and distribution analysis. Front. Physiol. 4 (1), 1–16. https://doi.org/10.3389/fphys.2013.00001.

Rugani, B., Caro, D., 2020. Impact of COVID-19 outbreak measures of lockdown on the Italian Carbon Footprint. Sci. Total Environ. 737, 139806. https://doi.org/10.1016/j.scitotenv.2020.139806.

Scheffer, M., Carpenter, S.R., Lenton, T.M., Bascompte, J., Brock, W., Dakos, V., van de Koppel, J., van de Leemput, I.A., Levin, S.A., van Nes, E.H., Pascual, M., Vandermeer, J., 2012. Anticipating critical transitions. Science 338, 344–348. https://doi.org/10.1126/science.1225244.

Sharma, S., Zhang, M., Anshika Gao, J., Zhang, H., Kota, S.H., 2020. Effect of restricted emissions during COVID-19 on air quality in India. Sci. Total Environ. 728, 138878. https://doi.org/10.1016/j.scitotenv.2020.138878.

Sterman, J.D., 2011. Communicating climate change risks in a skeptical world. Clim. Chang. 108, 811–826. https://doi.org/10.1007/s10584-011-0189-3.

Sterman, J.D., Sweeney, L.B., 2007. Understanding public complacency about climate change: adults' mental models of climate change violate conservation of matter. Clim. Chang. 80, 213–238. https://doi.org/10.1007/s10584-006-9107-5.

Tans and Keeling, 2020. Data From the Global Monitoring Laboratory by Dr. Pieter Tans, NOAA/GML (www.esrl.noaa.gov/gmd/ccgg/trends/) and Dr. Ralph Keeling. Scripps Institution of Oceanography scrippsco2.ucsd.edu. (Accessed 30 December 2020).

Tobías, A., Carnerero, C., Reche, C., Massagué, J., Via, M., Cruz Minguillón, M., Alastuey, A., Querol, X., 2020. Changes in air quality during the lockdown in Barcelona (Spain) one month into the SARS-CoV-2 epidemic. Sci. Total Environ. 726, 138540. https://doi.org/10.1016/j.scitotenv.2020.138540.

Tollefson, J., 2021. COVID curbed 2020 carbon emissions – but not by much. Nature 589, 343. https://doi.org/10.1038/d41586-021-00090-3.

Turner, A.J., Kim, J., Fitzmaurice, H., Newman, C., Worthington, K., Chan, K., Wooldridge, P.J., Köehler, P., Frankenberg, C., Cohen, R.C., 2020. Observed impacts of COVID-19 on urban $CO_2$ emissions. Geophys. Res. Lett. 47. https://doi.org/10.1029/2020GL090037 e2020GL090037.

Vaccari, F.P., Gioli, B., Toscano, P., Perrone, C., 2013. Carbon dioxide balance assessment of the city of Florence (Italy), and implications for urban planning. Landsc. Urban Plan. 120, 138–146. https://doi.org/10.1016/j.landurbplan.2013.08.004.

Vardag, S.N., Hammer, S., Levin, I., 2016. Evaluation of 4 years of continuous $\delta^{13}C(CO_2)$ data using a moving Keeling plot method. Biogeosciences 13, 4237–4251. https://doi.org/10.5194/bg-13-4237-2016.

Venturi, S., Tassi, F., Cabassi, J., Gioli, B., Baronti, S., Vaselli, O., Caponi, C., Vagnoli, C., Picchi, G., Zaldei, A., Magi, F., Miglietta, F., Capecchiacci, F., 2020. Seasonal and diurnal variations of greenhouse gases in Florence (Italy): inferring sources and sinks from carbon isotopic ratios. Sci. Total Environ. 698, 134245. https://doi.org/10.1016/j.scitotenv.2019.134245.

Vickers, D., Mahrt, L., 1997. Quality control and flux sampling problems for tower and aircraft data. J. Atmos. Ocean. Technol. 14 (3), 512–526. https://doi.org/10.1175/1520-0426(1997)014<0512:QCAFSP>2.0.CO;2.

Wang, Q., Lu, M., Bai, Z., Wang, K., 2020. Coronavirus pandemic reduced China's $CO_2$ emissions in short-term, while stimulus packages may lead to emissions growth in medium- and long-term. Appl. Energy 278, 115735. https://doi.org/10.1016/j.apenergy.2020.115735.

Webb, E.K., Pearman, G.I., Leuning, R., 1980. Correction of flux measurements for density effects due to heat and water vapour transfer. Q. J. R. Meteorol. Soc. 106 (447), 85–100. https://doi.org/10.1002/qj.49710644707.

Widory, D., Javoy, M., 2003. The carbon isotope composition of atmospheric $CO_2$ in Paris. Earth Planet. Sci. Lett. 215, 289–298. https://doi.org/10.1016/S0012-821X(03)00397-2.

Wu, S., Zhou, W., Xiong, X., Burr, G.S., Cheng, P., Wang, P., Niu, Z., Hou, Y., 2021. The impact of COVID-19 lockdown on atmospheric $CO_2$ in Xi'an, China. Environ. Res. 197, 111208. https://doi.org/10.1016/j.envres.2021.111208.

Zambrano-Monserrate, M.A., Ruano, M.A., Sanchez-Alcalde, L., 2020. Indirect effects of COVID-19 on the environment. Sci. Total Environ. 728, 138813. https://doi.org/10.1016/j.scitotenv.2020.138813.

Zimnoch, M., 2009. Stable isotope composition of carbon dioxide emitted from anthropogenic sources in the Kraków region, Southern Poland. Nukleonika 54 (4), 291–295.